IOP Publishing Journal of Physics: Condensed Matter
J. Phys.: Condens. Matter **31** (2019) 214004 (9pp) https://doi.org/10.1088/1361-648X/ab0822

Hydrogel micromotors with catalyst-containing liquid core and shell

Hong Zhu[1], Saraf Nawar[2], Jörg G Werner[2], Jinrun Liu[1], GaoShan Huang[1], YongFeng Mei[1], David A Weitz[2,3] and Alexander A Solovev[1,2]

[1] Department of Materials Science, 220 Handan Road, Fudan University, Shanghai 200433, People's Republic of China
[2] John A. Paulson School of Engineering and Applied Sciences, Harvard University, Cambridge, MA 02138, United States of America
[3] Department of Physics, Harvard University, Cambridge, MA 02138, United States of America

E-mail: solovevlab@gmail.com and weitz@seas.harvard.edu

Received 18 November 2018
Accepted for publication 18 February 2019
Published 21 March 2019

Abstract

Methacrylic anhydride-derived hydrogel microcapsules have unique properties, including reversibly tunable permeation, purification, and separation of dissolved molecular species. Endowing these dynamic encapsulant systems with autonomous motion will significantly enhance their efficiency and applicability. Here, hydrogel micromotors are realized using complex water-in-oil-in-water double emulsion drops and oil-in-water emulsion drops from glass capillary microfluidics and subsequent photopolymerization. Three hydrogel micromotor strategies are explored: microcapsules with thin shells and liquid cores with dispersed catalytic Pt nanoparticles, as well as water-cored microcapsules and homogeneous microparticles selectively coated with Ti/Pt catalytic layers. Autonomous motion of hydrogel particles and capsules is realized in hydrogen peroxide solutions, where generated oxygen microbubbles propel the dynamically responsive micromotors. The micromotors are balanced by weight, buoyancy, lateral capillary forces and show specific autonomous behaviours that significantly extend short range dynamic responses of hydrogels. Drop-based microfluidics represent a paradigm shift in the integration of multifunctional subsystems and high-throughput design of chemical micromachines in reasonable quantities towards their desired biomedical, environmental and flow/diffusion microreactor applications.

Keywords: micromotor, catalyst, autonomous, dynamic, responsive, hydrogel

Supplementary material for this article is available online

(Some figures may appear in colour only in the online journal)

1. Introduction

The field of nano- and micromotors that evolved mainly over the last decade is still in its infancy. The systems, often referred to as man-made nano-/micromachines, chemistry in motion, bio-inspired chemo-mechanical-systems or dynamic nanotechnology, explore numerous advantages of materials' dynamic functions [1–3]. Miniaturization in the machine design leads to multiple improvements of machine performance including negligible inertia, higher surface to volume ratio, higher strength to weight ratio, higher volumetric energy density, higher efficiency, faster relative motion by body lengths and ultra-precise movements by nano-/micro-steps [4]. It is crucial that micromotors can outswim the high viscosity of fluids at low Reynolds numbers [5]. Biological systems utilize efficient catalytically-powered nanoscale machines that can transport cargo faster than diffusion, actuate muscles and move cells [6]. More than a decade ago, several motive mechanisms were discovered to propel non-biological catalytic nano-/microparticles in fuel solutions using physical forces

and chemical gradients, namely self-electrophoresis, self-diffusiophoresis, dynamic surface tension and gas/bubble recoil [7]. Self-propelled autonomous nano-/micromotors consisting of different materials, sizes and shapes, such as micro-/nanorods [2, 3], tubes [8, 9], and spheres [10], have been demonstrated. Fundamentally, active enzymes at the single molecule and collective level can transduce enough force to self-propel, which may shed light on better understanding of active living matter and mechanobiology [11]. Nano/-micromotors have a broad scope of potential on-chip, *in vitro* and *in vivo* applications. For instance, in the biomedical field, self-powered nano/-micromotors can enhance delivery of drugs [12–16], isolation of cancer cells [17], perform single cell microsurgery [18] biosensing in motion, diagnostics and immunoassay analysis [19–21]. Moreover, a specific tumour-treating nanomedicine that triggers *in situ* catalytic reactions represents a new promising research direction [22, 23]. Dynamic nano-/micromotors are attracting considerable interest for decontamination of pollutants, removal of oil droplets, heavy metals and organic compounds [24–31]. Traditional water cleaning materials, such as iron [32], manganese oxide [33], metal organic framework (MOF) [34], activated carbon, graphene [35–37], and magnetic oleic acid-coated particles [38] are assembled with nano/-micromotors for environmental remediation and purification of water.

Recently, novel bioinspired and self-assembly methods of micromotors fabrication have been widely adopted [39, 40]. Catalytic nanoparticles incorporated in the membrane of Janus capsules [41], layer-by-layer polyelectrolytes with cross-linking of catalytic particles and enzymes [42], one step emulsification-solidification of oil-in-water (O/W) droplets [43] and folding of polymersomes into stomatocytes with encapsulated proteins [44], have been realized. Microfluidic techniques can be applied to compartmentalize the inner space of drops and generate multi-component double emulsions [45]. In response to external stimuli, such as pH, electric field and temperature, hydrogels can change their permeability, absorb large amounts of water, and swell for applications in forward osmosis, desalination, removal of pollutants, biohazardous threats, food industry, cosmetics, optics, pharmaceutics and tissue engineering [46]. However, despite of broad studies of hydrogels with local responsive properties, only several reports investigate autonomously motile hydrogels, which can swim over long distances [47–49].

In this study, we explore methacrylic anhydride-based chemistry to fabricate hydrogel micromotors consisting of microcapsules with catalyst-containing liquid cores (Pt-in-Caps), hydrogel Janus capsules with e-beam evaporated Pt catalyst (Pt-on-Caps), as well as homogeneous Janus particles with e-beam evaporated Pt catalyst (Pt-on-Gel). Micro/-particles and capsules are generated using mixtures of the hydrophobic monomers methacrylic anhydride (MAAn) and ethylene glycol dimethacrylate (EGDMA) and complex emulsion drop templating: water-in-oil-in-water (W/O/W) double emulsions and O/W single emulsion drops generated by a glass capillary microfluidic technique [50]. After photo-polymerization, hydrophobic poly(methacrylic anhydride) capsules are hydrolyzed to create permeable and pH-responsive hydrogel structures. Catalysts are either encapsulated in the liquid core during the formation of capsules or evaporated externally on the dry capsules/particles in vacuum using e-beam deposition. If a loaded liquid cargo contains carriers larger than the nanoporous openings in the shell, the carriers remain inside the capsule [50]. Moreover, hydrogel capsules can potentially operate as chemical flow/diffusion microreactors: reactants diffuse into the liquid core, where a catalytic reaction takes place, followed by the diffusion of the reaction products outside the microcapsule. When hydrogel micromotors with a Pt-catalyst are immersed in hydrogen peroxide solution a rapid growth and ejection of oxygen microbubbles is observed. In this report, we examine O_2-bubble propelled micromotors with specific dynamic responses, oxygen generation rates, different architectures (capsule, particle) and positions of the catalyst (liquid core, outer surface).

2. Experimental details

2.1. Materials

MAAn, EGDMA, Poly (vinyl alcohol) (Mw 13 000–23 000, 98% hydrolysed, PVA), aqueous hydrogen peroxide (H_2O_2, 30 wt%), rhodamine B (Sigma-Aldrich) and the platinum nanoparticles with 70 nm diameter (Sigma-Aldrich) were purchased and used as received. The hydrophilic 2-(methoxy-(polyethyleneoxy)propyl) trimethoxysilane and the hydrophobic trichloro(octadecyl)silane were purchased from Gelest and Sigma Aldrich, respectively. To test the motion of the micromotors two solutions were prepared: (i) a mixture composed of hydrogen peroxide (30% v/v aqueous solution), VWR® SoftCIDE®-NA Hand Soap (sol. A) and (ii) a mixture of hydrogen peroxide, propylene carbonate (sol. B).

2.2. Glass capillary microfluidic device

The microfluidic glass capillary devices are composed of two tapered round capillaries aligned in a square capillary, as shown in the figure 1. The smaller tapered round capillary works as the inlet and the larger tapered round capillary works as the collection outlet. An additional capillary pulled using a butane torch is inserted in the inlet capillary to inject the core liquid. The tip of the collection capillary has approximately twice the diameter than the tip of the inlet capillary. The surface of the round outlet glass capillary was treated by 2-(methoxy-(polyethyleneoxy)propyl) trimethoxysilane to maintain the hydrophilicity. The inlet capillary was treated with trichloro(octadecyl)silane to create hydrophobic surfaces. Both capillaries were treated for one hour, followed by removal of the silanes with an air jet and assembly of the glass capillary microfluidic device.

2.3. Hydrogel microparticles and microcapsules

MAAn (98 mol%) and EGDMA (2 mol%) are mixed together and degassed with nitrogen for 15 min. Just before the microfluidic fabrication, 1 mol% 2-Hydroxy-2-methylpropiophenone (Darocure 1173) photo-initiator is mixed with monomers to

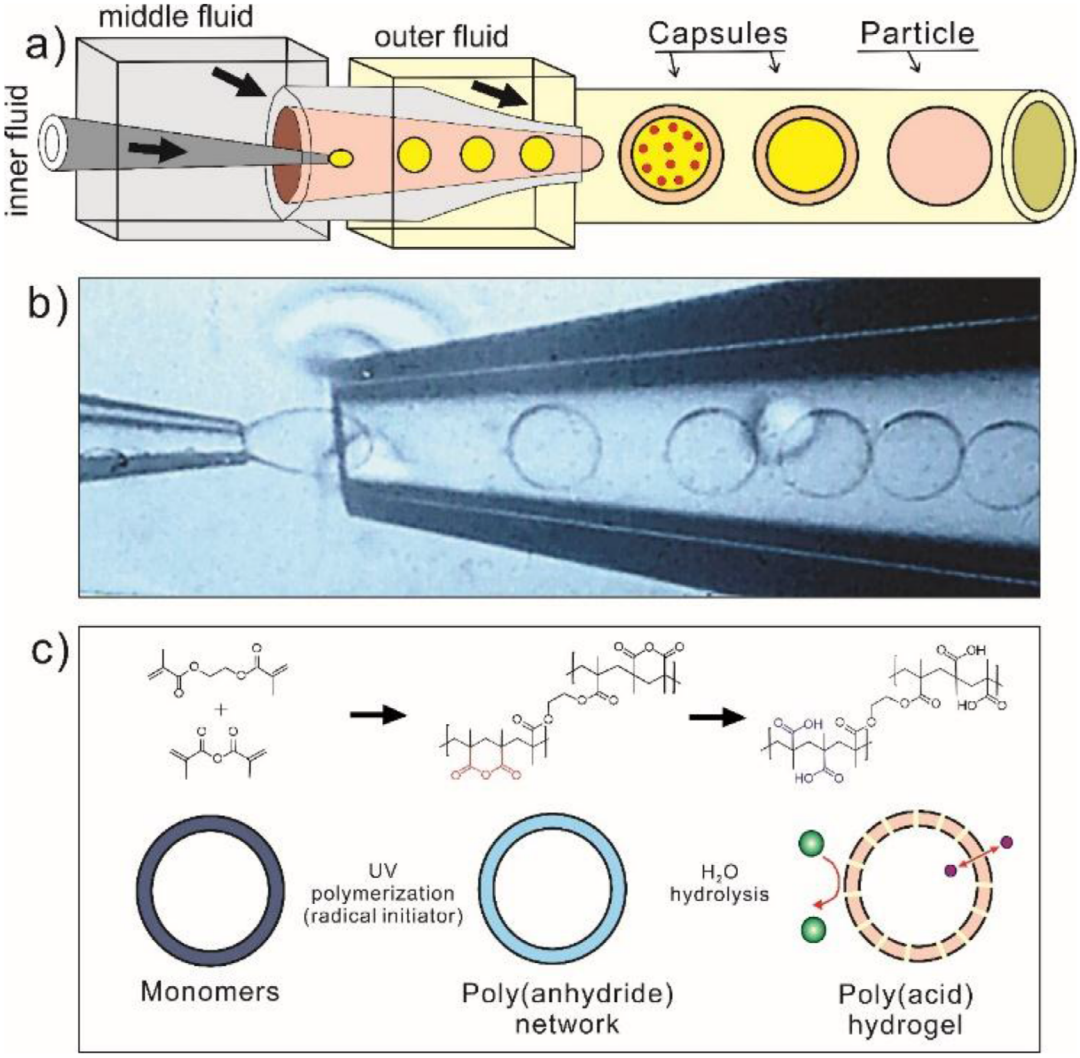

Figure 1. Generation of three types of hydrogel micromotors consisting of hydrogel capsules and particles. (a) Schematic of microfluidic glass capillary device used for the generation of hydrogel particles and capsules from complex emulsion drops. (b) Optical microscopy image of double emulsion drop formation in glass capillary microfluidic device. After generation, the double emulsions are irradiated with UV light (not shown) to photo-polymerize the shells of the microcapsules and particles. (c) Anhydride chemistry of hydrogel capsule shells formed from W/O/W double emulsion drops and schematic permeation selectivity test of the shell using differently sized fluorescent dyes.

create the water-immiscible monomer solution. The aqueous phases (inner and outer) contain 5 wt % PVA as a stabilizing surfactant, optionally with Platinum nanoparticles for Pt-laden microcapsules. To generate hydrogel microparticles only the middle and the outer fluid flows are used to generate O/W emulsion drops. For the formation of hydrogel microcapsules, the inner aqueous, middle monomer, and outer aqueous fluids are pumped simultaneously through the microfluidic device at rates in ranges 1000–3000, 3000–10 000, and 7000–12 000 μl h^{-1}, respectively. The emulsion drops are photo-crosslinked by exposure to UV-light (OmiCure S1500, 320–500 nm filter) for 15 min immediately after drop formation to obtain poly(methacrylic anhydride-co-ethylene glycol dimethacrylate) microcapsules and particles. Microcapsules are hydrolyzed in a buffer solution at pH 11 over 24 h to create hydrophilic and permeable poly(methacrylic acid) hydrogel shells. Particles and hydrolysed capsules without Pt nanoparticles loadings are dried on a glass slide in a desiccator and used for electron-beam evaporation of catalytic Ti/Pt layer. The deposition of thin Ti/Pt films with e-beam evaporation is done directly on the hydrogel particles after photo-polymerization without prior hydrolysis. Titanium thin films are deposited before platinum for a better adhesion of the platinum layer to the hydrogel surface of the capsules and particles. After this, catalyst-coated capsules are reimmersed in solution, where they hydrate and restore their spherical shape in a few minutes.

3. Results and discussion

Three architectures of hydrogel micromotors are explored in this study: (i) microcapsules with Pt nanoparticles-containing liquid cores (Pt-in-Caps) from photo-polymerized W/O/W double emulsions, (ii) microcapsules with liquid cores and e-beam coated Ti/Pt (10/10 nm) catalytic layers (Pt-on-Caps) and (iii) hydrogel particles with coated Ti/Pt

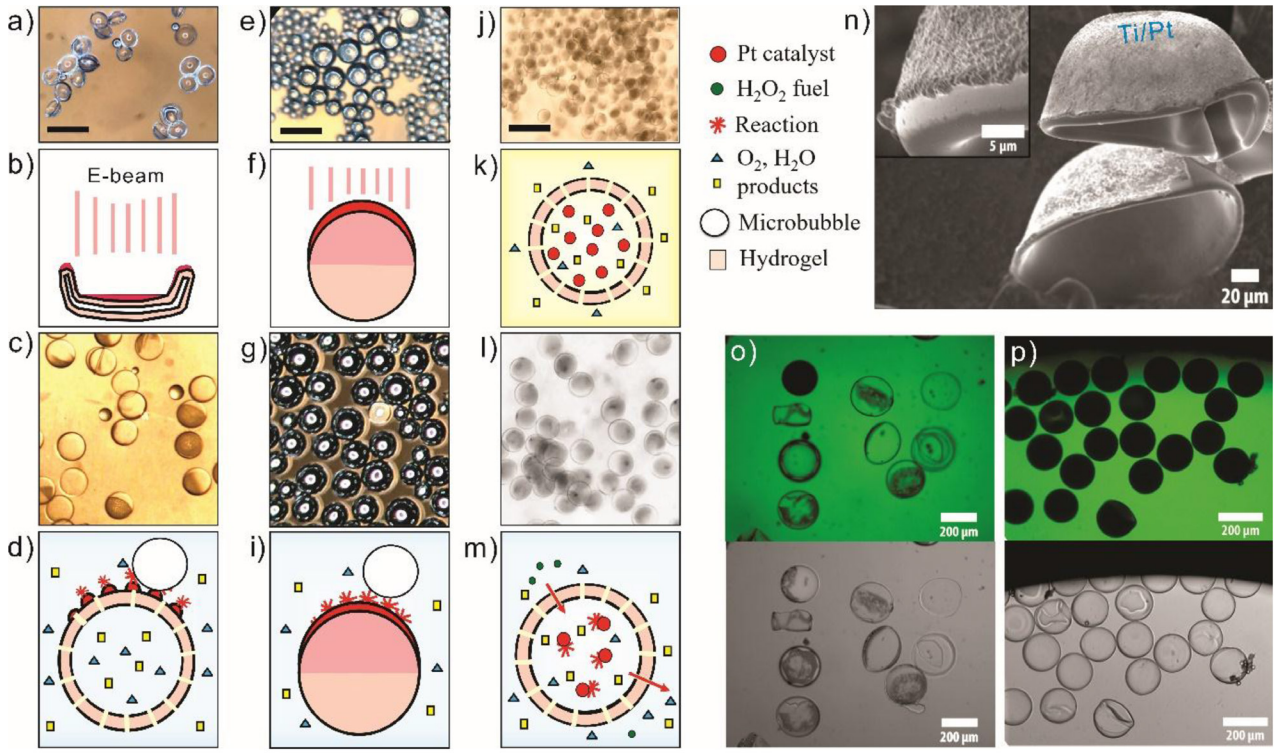

Figure 2. Preparation of hydrogel micromotors with catalytic liquid core and shell. (a) Optical microscopy image of dry capsules after photo-polymerization. The scale bar is 350 μm. (b) Schematic of e-beam evaporation of Ti/Pt thin film on dry capsules. (c) Unbuckled capsules immersed in aqueous fluid that restores their spherical shape due to permeation of water molecules through the hydrogel shell. (d) Schematic of unbuckled Janus particles generating oxygen bubble in chemical fuel. (e) Optical microscopy image of dry hydrogel particles, followed by (f) the e-beam deposition of Ti/Pt catalyst, (g) drying of particles in the air and (i) schematic of catalytic Janus particles located in the chemical fuel solution. The scale bar is 350 μm. (j) Optical microscopy image of photo-polymerized capsules with 70 nm diameter catalytic nanoparticles direclty encapsuled in aquoeus liquid core during generation of W/O/W double emulsions. The scale bar is 480 μm. (k) Schematic of individual capsule with nanoparticles and permeable shells, (l) capsules with NPs after cleaning in water and (m) schematic of catalytic reaction in the liquid core of capsule. (n) Scanning electron microscopy of dry capsules with evaporated Ti/Pt catalysts. (o) and (p) Confocal laser scanning fluorescence (top) and bright field (bottom) images of microcapsules after (o) and before (p) drying and e-beam evaporation of Ti/Pt thin films, demonstrating the change in permeability during the procedure. The capsules are challenged with FITC-dextran-500kDa.

layers (Pt-on-Gel) from photo-polymerized oil-in-water O/W emulsions. Two H_2O_2 fuel solutions were used to study the generation of oxygen bubbles and the resulting motion of the micromotors: a mixture of H_2O_2 and dish soap (for stabilization of microbubbles, Sol. A) and a mixture of H_2O_2 and propylene carbonate (for reduction of lifetime of microbubbles, Sol. B). All three types of micromotors powered by catalytic reactions show specific long range dynamic responses due to interactions consisting of micromotors' weight, buoyancy, motive and capillary forces. Figure 1(a) shows a schematic of the fabrication process of hydrogel micro- particles and capsules using single O/W emulsion drops and double emulsion W/O/W drop templating techniques, respectively. When the inner, middle and outer fluid flows are used, microcapsules are generated. Pt nanoparticles are injected in the inner liquid core of the capsules to obtain Pt-in-Caps micromotors. If only middle and outer fluid flows are used, homogeneous hydrogel particles are formed. Figure 1(b) shows an optical microscopy image of the generation of W/O/W double emulsion drops. Figure 1(c) shows the chemical conversion of W/O/W double emulsion drops with monomer shells to poly(anhydride) microcapsules, followed by the hydrolysis to microcapsules with thin poly(acid) hydrogel shells.

Figure 2 illustrates our design of hydrogel micromotors with different architectures and positions of catalysts for controllable chemical reactions, diffusion of reaction products and nucleation of O_2 bubbles. Figures 2(a)–(i) shows the preparation of hydrogel capsules and particles with evaporated thin Ti/Pt layers on dry hydrogels using e-beam. The microcapsules buckle during drying and only one side of the capsule is exposed for metal evaporation. When reimmersed in an aqueous solution, the dry Janus Ti/Pt capsules unbuckle due to rehydration and restore their original spherical shape in minutes, as demonstrated in figures 2(c) and (d). Hydrogel Janus Ti/Pt particles, shown in figures 2(e)–(i), retain their spherical shape both in air and liquid environment. Figures 2(j)–(l) shows the transfer of the capsules containing Pt nanoparticles from the fabrication solution containing PVA (5% w/w) to a pH 11 aqueous solution to hydrolyze the hydrogel shell. Schematic drawings in figures 2(d), (i) and (m) indicate the micromotors in chemical fuels. Figure 2(n) shows SEM images of dried capsules with evaporated Ti/Pt catalyst. During e-beam evaporation, the permeability of the microcapsules increases slightly. Figures 2(o) and (p) shows a permeation test of the coated capsules with FITC-dextran-500 kDa indicating that only some capsules remain

impermeable to the dye after coating (the second row), as compared to dry capsules without Ti/Pt coating, which stay impermeable even to FITC-dextran-10 kDa. 500 kDa Dextran has a Stokes diameter around 29.4 nm. This indicates that the drying and e-beam evaporation disrupts the shell hydrogel networks somewhat.

3.1. Hydrogel capsule-based micromotor with a catalytic nanoparticle-containing liquid core

A feasible Pt-in-Caps micromotor configuration is based on a reaction and diffusion process, where reactants enter through the hydrophilic poly(methacrylic acid) hydrogel shell, react with the encapsulated catalyst and the reaction products diffuse outside the microcapsule.

Hydrolyzed hydrogel capsules allow trapping of catalytically active Pt nanoparticles (70 nm in diameter), due to their larger size than the capsule nanopores. Small molecules including water, hydrogen peroxide, and molecular oxygen can permeate through the hydrophilic shell. Upon transfer of the capsules with Pt NPs to a hydrogen peroxide solution, hydrogen peroxide diffuses through the capsule shell and decomposes into water and oxygen, according to the reaction $2\ H_2O_2 \rightarrow 2\ H_2O + O_2$. A liquid-core containing catalytic NPs is replaced by the rapidly growing gaseous core and O_2 microbubbles are trapped inside the microcapsules. The motility of Pt-in-Caps is expected due to a possible fluid pumping mechanism during catalytic activity. For instance, in biology myxobacteria glide by slime extrusion from the Junctional Pore Complex with the diameter of individual pore as small as 8 nm [51]. However, our experiments reveal that Pt-in-Caps remain static in hydrogen peroxide solutions probably due to a symmetric radial diffusion of reaction products or inability to achieve an efficient hydrodynamic pumping of fluid through the nanopores. In our current study, bubble growth inside the aqueous core of microcapsules is observed if concentrations of the hydrogen peroxide fuel is high enough (e.g. 10% v/v). However, such microbubbles can rapidly dissolve due to a high Laplace pressure. It is known that homogeneous nucleation of bubbles in solution requires higher energy than heterogeneous nucleation on surfaces. Moreover, an active growth of bubble requires continuous supply and accumulation of gas molecules, which in case of the thin shell hydrogel capsules, can escape outside the permeable hydrogel shells. A recent study proves that increased roughness, surface defects or microcavity in the poly(ethylene glycol) diacrylate (PEGDA) hydrogel micromotors are required for pinning of O_2 bubbles and leading to an autonomous propulsion [48]. Since active swimming of micromotors requires a constant ejection of bubbles, defects in the shell of hydrogel capsules are created by pressing the capsules using metallic tweezers (video 1 of the electronic supplementary information (ESI), available online at stacks.iop.org/JPhysCM/31/214004/mmedia), shown in figure 3(a). As a result, a fast growth of O_2 bubbles in the partially ruptured capsules is observed. Moreover, when the O_2 microbubble fully fills the microcapsule, it replaces the liquid with a gaseous core and strong attraction to the Petri dish edge is observed by lateral capillary force (i.e. meniscus climbing effect) due to a concave shape of the air-liquid interface near the edge of the Petri dish (video 2, ESI). The capillary force acts over long range and it can be simplified to the following equation $F_c \approx \gamma R^2/L$, where R is the radius of the air-fluid curvature, L is the characteristic length scale of the interaction, and γ is the surface tension of the solution. Capillary length is determined by equation $\lambda_c = \sqrt{\gamma/\rho g}$, where g is the gravitational acceleration and ρ is the density of the fluid (accepting water surface tension $72.8 \cdot 10^{-3}$ N m^{-1} and the density of water 10^3 kg m^{-3}—the capillary length is 2.72 mm). Schematic of the microcapsule with a gaseous core, acting forces (buoyancy, weight, capillary and motive) and optical microscopy sequences of capsule-based micromotors attracted to a Petri dish wall are shown in figure 3(b). In a similar study, motion of metallic micro-caps is achieved using solid shelled hollow spherical micromotors [52]. It is revealed that an efficient supply of hydrogen peroxide fuel can take place through the microscopic opening and the fluidic gap between the bubble surface and the catalytic walls. Thus, responsive Pt-in-Caps with gas cores can be used to probe capillary interactions, while Pt-in-Caps with liquid cores represent a novel platform for molecular separation and encapsulation of chemical species.

3.2. Hydrogel capsule-based micromotors with coated catalyst

Evaporation of Ti/Pt films on dried microcapsules is used to obtain Pt-on-Caps micromotors with a catalyst layer exposed to the outside surface of capsules. Upon re-immersion in aqueous liquids, the Janus Pt-on-Caps restore their spherical shape and the core is re-filled by the aqueous solution. Pt-on-Caps exhibit a higher catalytic activity and faster speeds of motion than Pt-in-Caps. Figure 3(c) shows one individual Janus microcapsule self-propelled by producing oxygen bubbles on its surface (Sol. B, H_2O_2 10% v/v). The Pt-on-Caps is propelled during bubble nucleation, growth and recoil (video 3, ESI). The mechanism of motion of Pt-on-Caps is similar to bubble-propelled catalytic shell micromotors considered before in details [52]. The motive force of Pt-on-Caps at low Reynolds number can be approximated by the Stokes drag force $F_m = 6\pi\mu Rv$, where v is the velocity of the micromotor, μ is the fluid viscosity, and R is the bubble radius. Accepting an average micromotor speed of 100 μm s^{-1}, a solution viscosity of 8.90×10^{-4} Pa and the radius of Pt-on-Caps micromotor 75 μm, the estimated force of the micromotors is on the order of 15 pN. If relatively large microbubbles are generated, comparable to the micromotor size, the motive force of the Pt-on-Caps is sufficient to swim fast and deliver a potential cargo. Hydrogel capsules that stay in water for a while (~10 d) can be fully hydrolysed. However, due to the challenge of coating buckled capsules in vacuum, a relatively low number of capsules achieved a half hemisphere of catalytic Ti/Pt coatings using e-beam evaporation. Presumably, the e-beam evaporation and a subsequent immersion in an aqueous solution cause damage to the hydrogel membrane.

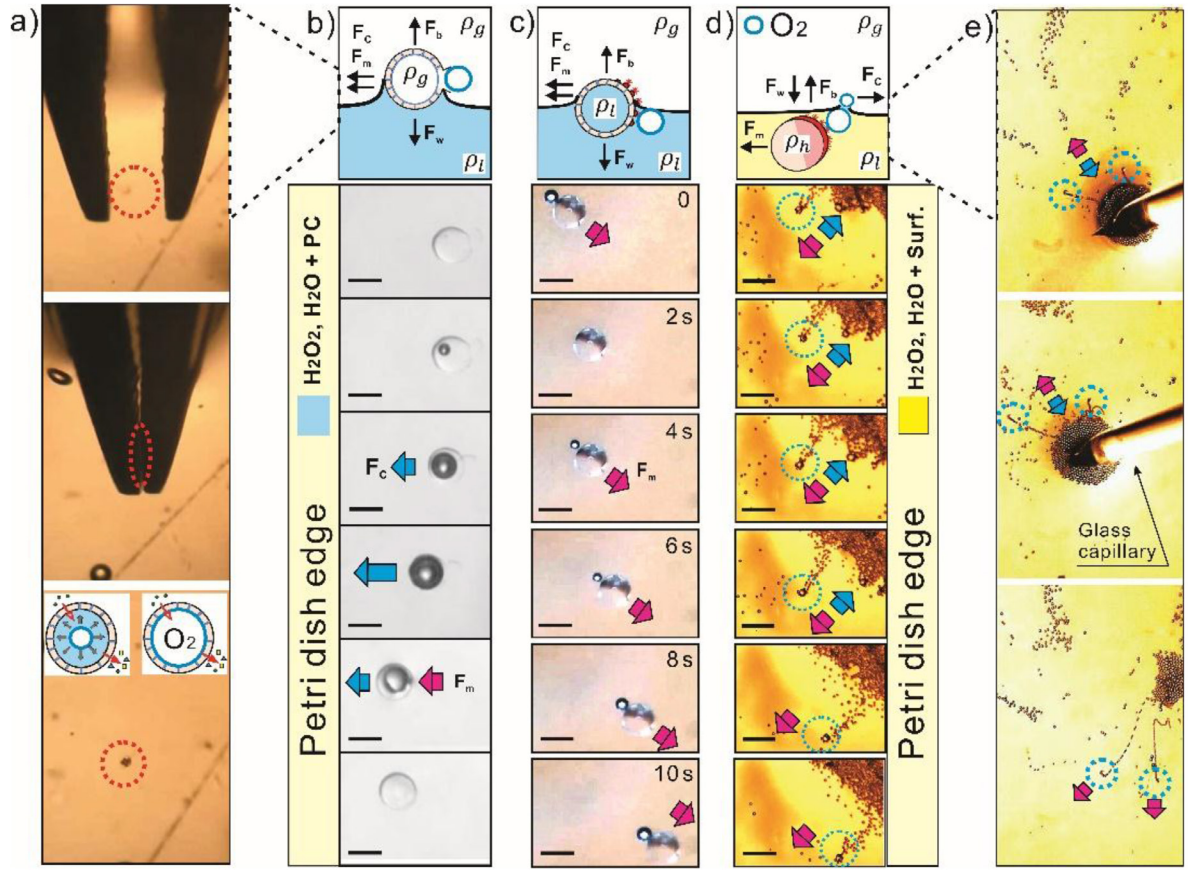

Figure 3. Dynamics of hydrogel micromotors balanced by the forces: weight (F_w), buoyancy (F_b), lateral capillary (F_c) and motive (F_m). (a) Metallic tweezers enabled mechanical actuation of microcapsules with liquid catalytic nanoparticles-containing cores to create shell opening and enhance generation of oxygen microbubbles during the catalytic reaction of hydrogen peroxide decomposition. Inset schematic shows growth of an oxygen bubble in a microcapsule. (b) Schematic and optical miroscopy image sequences of oxygen bubble growth and ejection from microcapsules with Pt nanoparticles-containing liquid cores. The scale bar is 200 μm. (c) Schematic and optical microscopy image sequence of a self-propelled microcapsule with externally coated Ti/Pt thin film. Red arrows show the direction of microcapsule motion. The scale bar is 200 μm. (d) Schematic and optical microscopy image sequence of self-propelled hydrogel particles with coated catalysts. Blue arrows indicate the attractive lateral capillary force acting on an individual moving particle-based micromotor that generates many bubbles. Red arrows indicate motive forces of autonomous micromotors. The scale bar is 650 μm. (e) Optical micrograph demonstrating a glass capillary inserted at the air-liquid interface causes self-alingment of the hydrogel particle micromotors and autonomous repulsion.

3.3. Hydrogel particle-based micromotors with coated catalyst

Figure 3(d) shows a schematic of hydrogel Janus micromotors with evaporated Ti/Pt catalyst and optical microscopy sequences of self-propelled Pt-on-Gel micromotors (Sol. A, H_2O_2 10% v/v). In contrast to other types of micromotors, Pt-on-Gel self-propel faster, detect fluidic meniscus, self-align and repel from the attractive capillary force, i.e. Petri dish edges or external glass capillary inserted at the liquid-air interface (video 4, ESI). We hypothesize that such self-alignment behavior of Pt-on-Gel is due to interaction between the O_2 gas bubbles and the hydrogel particle. The density of the hydrogel is higher than water and it is observed that Pt-on-Gel micromotors placed in aqueous solutions without fuel rapidly sink. O_2 bubbles bring the Pt-on-Gel to the air-liquid interface, while O_2 experience a higher buoyancy and thus, a more attractive lateral capillary force is acting on the O_2 bubbles in the concave liquid meniscus. In our view, since the O_2 bubbles and the micromotors are connected for microseconds, such tandems self-repel from an attractive capillary force, i.e. solid edges. Interesting, while most of the micromotors remain in balance, some smart Pt-on-Gel generate bubbles at a faster rate and outswim the capillary distance (video 5, ESI). Figure 3(e) shows one example of such a dynamic interaction of two Pt-on-Gel micromotors with an external glass capillary at the air-liquid interface. After the glass capillary is removed from the solution interface, the micromotors continue to swim in the initial directions of their motive forces.

3.4. Comparison among hydrogel micromotors

Water-filled Pt-in-Caps and Pt-on-Caps micromotors have a smaller fraction of the denser hydrogel because of the large water content in the core compared to the thin hydrogel shell. Hence, homogeneous Pt-on-Gel micromotors have a higher overall density. Due to a larger weight to buoyancy ratio, particle-based micromotors rapidly sink in solutions without fuel. A larger buoyancy of Pt-in-Caps with gaseous core leads to a new behaviour at the air-liquid interface similar to

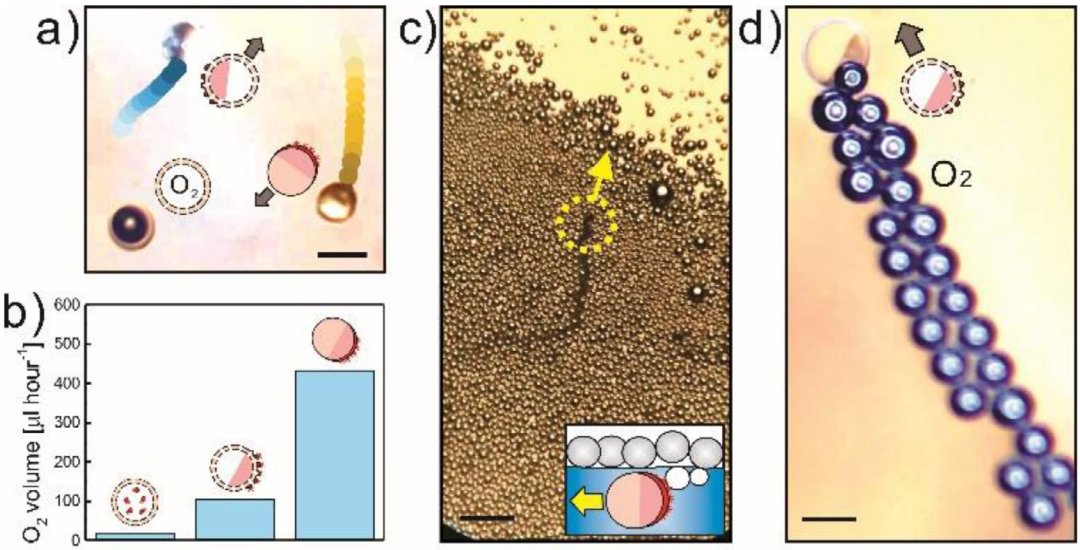

Figure 4. Motion of hydrogel micromotors in hydrogen peroxide solutions and micromotors-enabled generation of oxygen gas. (a) Tracked trajectories of Pt-in-Caps, Pt-on-Caps and Pt-on-Gel micromotors (sol. B, 10% v/v H_2O_2). Inset images show schematic of micromotors and their direction of motion. The scale bar is 200 μm. (b) Micromotors enbled generation of oxygen gas in 10% v/v H_2O_2 (sol. A). (c) Optical micrograph showing the motion of individual Pt-on-Gel micromotor through an oxygen microbubble raft. Inset shows Pt-on-Gel micromotor moving efficiently under oxygen bubble raft. The scale bar is 650 μm. (d) Optical micrograph of long comet tails of O_2 bubbles generated by an individual Pt-on-Caps micromotor (sol. A, 5% v/v H_2O_2). The scale bar is 150 μm.

conventional gas bubbles, where a strong capillary attraction to solid edges is observed. The surfactants in Sol. B are known to reduce surface tension and stabilize microbubbles, typically long elongated comet tails can be observed for micromotors in surfactant-containing solutions of hydrogen peroxide. While in Sol. B, microbubbles break immediately after generation, which helps to eliminate the accumulation of O_2 bubbles that otherwise can block the motion of micromotors. Figure 4(a) shows trajectories of the self-propelled motion of Pt-on-Caps and Pt-on-Gel micromotors (Sol. A, H_2O_2 10% v/v), while Pt-in-Caps filled with gaseous core remain static. Pt-on-Gel are the fastest micromotors self-propelling up to 135 μm s^{-1} due to an efficient bubble recoil and acceleration by bubble comet tails. Pt-on-Caps move with an average speed of 68 μm s^{-1}. Pt-on-Caps move slower than Pt-on-Gel due to a catalytic layer delamination during the unbuckling process of Janus capsules. Pt-in-Caps do not self-propel without mechanical activation and defects in the hydrogel shell are required. However, a rapid growth of O_2 bubble in the Pt NPs containing liquid core can be achieved. Figure 4(b) shows the O_2 gas generation rate of the different types of hydrogel micromotors: Pt-in-Caps, Pt-on-Caps and Pt-on-Gel: 18, 105 and 432 μl h^{-1}, respectively (Sol. A, H_2O_2 10% v/v). Since surfactants reduce surface tension of aqueous fuels the generation of O_2 microbubbles can be substantially enhanced. Moreover, Pt-on-Gel micromotors self-propel efficiently through microbubble rafts, shown in figure 4(c). If a micromotor is located below the surface of the liquid, it can effectively overcome accumulated O_2 bubble raft barriers.

Figure 4(d) shows an individual Pt-on-Caps micromotor self-propelled by a long O_2 bubble comet tail (Sol. A, H_2O_2 5% v/v). In our view, Pt-in-Caps micromotors can have another important function beyond motion. In many processes, biological cells rely on a transport of smaller molecules through membrane by diffusion, while keeping larger fluidic subsystems constantly in the fluidic core and at the same time employing biological nanomotors to overcome diffusion. According to the Stokes–Einstein equation the diffusion of a nanoparticle can be estimated from the following equation $D = TK_b/3\pi\mu r$, where T is the absolute temperature, K_b is the Boltzmann's constant, μ is the dynamic viscosity and r is the radius of the spherical particle. Another important parameter includes mixing time of nanoparticles $t_{mix} = d_c^2/D$, where d_c is the diameter of the capsule and D is the diffusion coefficient. It can be theoretically estimated how often nanoparticles can collide in a fluidic micromotor $t_{traffic} = d_c^3/Dr$ [4]. For instance, for a spherical Pt NPs with 70 nm diameter, estimated diffusion coefficient is on the order of 10^{-12} m^2 s^{-1}. Assuming a microcapsule diameter equal to 100 μm, the mixing time is on the order of seconds and traffic time is on the order of tens of days for Pt-in-Caps. Remarkably, typical mixing and traffic time in biological cells is within milliseconds that can provide insight into future design of man-made microfluidic micromachines.

4. Conclusions

In this report, hydrogel micromotors with catalyst-containing liquid core and shell are presented. Balances of weight/buoyancy, motive power/capillary forces of Pt-in-Caps, Pt-on-Caps and Pt-on-Gel micromotors lead to specific dynamic behaviours found for each type of micromotors in the hydrogen peroxide fuel solutions. The fastest speed is observed for Pt-on-Gel micromotors, which is attributed to more efficient

catalytic coating during e-beam deposition. Pt-on-Caps micromotors can generate a sufficient motive force to carry a potential cargo. While, for Pt-in-Caps micromotors, stable nucleation, growth and generation of oxygen bubbles require defects in the hydrogel shell. However, essentially and fundamentally, key parameters for Pt-in-Caps are controllable permeability, purification, separation, reaction and conversion of particles and molecules. Pt-in-Caps micromotors can potentially contain ultra-high surface area nanoparticles to filter, adsorb, capture, react, separate molecular species and decontaminate heavy metals, organic pollutants in water. Since nano/-micromotors themselves represent particulate pollutants, nanoparticle-laden composites, i.e. nanoparticles embedded in particles/capsules, can be particularly useful to construct a purification device [53]. Moreover, microfluidics can further strengthen fabrication of microdrops [54] and known principles can be applied to divide, add, mix and sort chemical micromachines at kHz rate. Ganti theoretically considered that biological cells operate by stirring, reaction, diffusion and active transport of their internal components in fluidic space free of geometrical constrains [55]. While approaching functionalities inherent to biomaterials microfluidic techniques offer a tremendous flexibility to explore man-made chemical micromachines with multifunctional subsystems.

Acknowledgments

AAS is deeply grateful for the young '1000 Talents' Plan from P. R. China. The authors acknowledge financial support from the Natural Science Foundation of China (grant no. 51475093). This work was in part supported by the National Science Foundation (DMR-1708729). This work was performed in part at the Harvard MRSEC (Grant No. DMR-1420570) and the Center for Nanoscale Systems (CNS), a member of the National Nanotechnology Coordinated Infrastructure Network (NNCI), which was supported by the National Science Foundation under NSF Award No. 1541959. CNS is part of Harvard University.

ORCID iDs

Jörg G Werner https://orcid.org/0000-0001-7845-086X
GaoShan Huang https://orcid.org/0000-0002-0525-7177
YongFeng Mei https://orcid.org/0000-0002-3314-6108
AlexanderA Solovev https://orcid.org/0000-0001-5918-3102

References

[1] Ismagilov R F, Schwartz A, Bowden N and Whitesides G M 2002 *Angew. Chem., Int. Ed. Engl.* **41** 652
[2] Ozin G A, Manners I, Fournier-Bidoz S and Arsenault A 2005 *Adv. Mater.* **17** 3011
[3] Paxton W F, Kistler K C, Olmeda C C, Sen A, Angelo S K S, Cao Y, Mallouk T E, Lammert P E and Crespi V H 2004 *J. Am. Chem. Soc.* **126** 13424
[4] Rogers B, Adams J and Pennathur S 2011 *Nanotechnology: Understanding Small Systems* 2nd edn (Boca Raton, FL: Taylor and Francis)
[5] Purcell E M 1977 *Am. J. Phys.* **45** 3
[6] Kolomeisky A B 2013 *J. Phys.: Condens. Matter* **25** 463101
[7] Ning H, Zhang Y, Zhu H, Ingham A, Huang G, Mei Y and Solovev A A 2018 *Micromachines* **9** 75
[8] Solovev A A, Mei Y, Ureña E B, Huang G and Schmidt O G 2009 *Small* **5** 1688
[9] Mei Y, Huang G, Solovev A A, Ureña E B, Mönch I, Ding F, Reindl T, Fu R K Y, Chu P K and Schmidt O G 2008 *Adv. Mater.* **20** 4085
[10] Gibbs J G and Zhao Y P 2009 *Appl. Phys. Lett.* **94** 163104
[11] Kanti Dey K, Dey K K and Sen A 2016 *Biophys. J.* **110** 546a
[12] Patra D, Sengupta S, Duan W, Zhang H, Pavlick R and Sen A 2013 *Nanoscale* **5** 1273
[13] Gao W and Wang J 2014 *Nanoscale* **6** 10486
[14] Peng F, Tu Y and Wilson D A 2017 *Chem. Soc. Rev.* **46** 5289
[15] Guix M, Mayorga-Martinez C C and Merkoçi A 2014 *Chem. Rev.* **114** 6285
[16] Ma X, Feng H, Liang C, Liu X, Zeng F and Wang Y 2017 *J. Mater. Sci. Technol.* **33** 1067
[17] Gao W, de Ávila B E-F, Zhang L and Wang J 2018 *Adv. Drug Deliv. Rev.* **125** 94
[18] Srivastava S K, Medina-Sánchez M, Koch B and Schmidt O G 2016 *Adv. Mater.* **28** 832
[19] Esteban-Fernández de Ávila B, Martín A, Soto F, Lopez-Ramirez M A, Campuzano S, Vásquez-Machado G M, Gao W, Zhang L and Wang J 2015 *ACS Nano* **9** 6756
[20] Chałupniak A, Morales-Narváez E and Merkoçi A 2015 *Adv. Drug Deliv. Rev.* **95** 104
[21] de Ávila B E-F, Zhao M, Campuzano S, Ricci F, Pingarrón J M, Mascini M and Wang J 2017 *Talanta* **167** 651
[22] Huo M, Wang L, Chen Y and Shi J 2017 *Nat. Commun.* **8** 357
[23] Lin H, Chen Y and Shi J 2018 *Chem. Soc. Rev.* **47** 1938
[24] Uygun D A, Jurado-Sánchez B, Uygun M and Wang J 2016 *Environ. Sci.* **3** 559
[25] Zhang Q, Dong R, Wu Y, Gao W, He Z and Ren B 2017 *ACS Appl. Mater. Interfaces* **9** 4674
[26] Xuan M, Lin X, Shao J, Dai L and He Q 2015 *Chem. Phys. Chem.* **16** 147
[27] Gao W and Wang J 2014 *ACS Nano* **8** 3170
[28] Srivastava S K, Guix M and Schmidt O G 2016 *Nano Lett.* **16** 817
[29] Chen A, Ge X H, Chen J, Zhang L and Xu J H 2017 *Lab Chip* **17** 4220
[30] Eskandarloo H, Kierulf A and Abbaspourrad A 2017 *Nanoscale* **9** 13850
[31] Safdar M, Simmchen J and Jänis J 2017 *Environ. Sci.* **4** 1602
[32] Teo W Z, Zboril R, Medrik I and Pumera M 2016 *Chem. A Eur. J.* **22** 4789
[33] Wani O M, Safdar M, Kinnunen N and Jänis J 2016 *Chemistry* **22** 1244
[34] Wang R, Guo W, Li X, Liu Z, Liu H and Ding S 2017 *RSC Adv.* **7** 42462
[35] Jurado-Sánchez B, Sattayasamitsathit S, Gao W, Santos L, Fedorak Y, Singh V V, Orozco J, Galarnyk M and Wang J 2015 *Small* **11** 499
[36] Orozco J, Mercante L A, Pol R and Merkoçi A 2016 *J. Mater. Chem.* A **4** 3371
[37] Vilela D, Parmar J, Zeng Y, Zhao Y and Sánchez S 2016 *Nano Lett.* **16** 2860
[38] Pan D, Mou F, Li X, Deng Z, Sun J, Xu L and Guan J 2016 *J. Mater. Chem.* A **4** 11768
[39] Wu Z, Lin X, Si T and He Q 2016 *Small* **12** 3080

[40] Wang H, Potroz M G, Jackman J A, Khezri B, Marić T, Cho N-J and Pumera M 2017 *Adv. Funct. Mater.* **27** 1702338
[41] Wang L, Liu Y, He J, Hourwitz M J, Yang Y, Fourkas J T, Han X and Nie Z 2015 *Small* **11** 3762
[42] Wu Y, Si T, Shao J, Wu Z and He Q 2016 *Nano Res.* **9** 3747
[43] Gao W, Liu M, Liu L, Zhang H, Dong B and Li C Y 2015 *Nanoscale* **7** 13918
[44] Abdelmohsen L K E A, Nijemeisland M, Pawar G M, Janssen G-J A, Nolte R J M, van Hest J C M and Wilson D A 2016 *ACS Nano* **10** 2652
[45] Adams L L A, Kodger, T E, Kim S-H, Shum H C, Franke T and Weitz D A 2012 *Soft Matter* **8** 10719
[46] Seliktar D 2012 *Science* **336** 1124
[47] Liang Y, Wang H, Yao D, Chen Y, Deng Y and Wang C 2017 *J. Mater. Chem.* A **5** 18442
[48] Keller S, Teora S P, Hu G X, Nijemeisland M and Wilson D A 2018 *Angew. Chem., Int. Ed. Engl.* **57** 9814
[49] Wang H, Gu X and Wang C 2016 *ACS Appl. Mater. Interfaces* **8** 9413
[50] Werner J G, Nawar S, Solovev A A and Weitz D A 2018 *Macromolecules* **51** 5798
[51] Wolgemuth C W and Oster G 2004 *J. Mol. Microbiol. Biotechnol.* **7** 72
[52] Huang W, Manjare M and Zhao Y 2013 *J. Phys. Chem.* C **117** 21590
[53] Khan M and Lo I M C 2017 *Hazard. Mater.* **322** 195
[54] Agresti J J, Antipov E, Abate A R, Ahn K, Rowat A C, Baret J-C, Marquez M, Klibanov A M, Griffiths A D and Weitz D A 2010 *Proc. Natl Acad. Sci. USA* **107** 4004
[55] Gánti T 2003 *The Principles of Life* (Oxford: Oxford University Press)